J Mater Sci (2019) 54:3368–3382

Materials for life sciences

A mechanically robust double-network hydrogel with high thermal responses via doping hydroxylated boron nitride nanosheets

Lu Xing[1], Chengxin Hu[1], Yulin Zhang[1], Xiangdong Wang[1], Lingying Shi[1], and Rong Ran[1,*]

[1] College of Polymer Science and Engineering, Sichuan University, Chengdu 610065, China

Received: 31 July 2018
Accepted: 15 October 2018
Published online: 22 October 2018

ABSTRACT

Double-network (DN) hydrogel which possesses many superior performances such as excellent toughness, viscoelasticity and self-healing ability has become promising biomaterials. However, lack of thermal conductivity and moderate adhesiveness has greatly limited their application as load-bearing cartilage substitutes. Boron nitride itself has good rigidity and thermal conductivity but poor water solubility. Hydroxylated boron nitride nanosheets (OH-BNNSs) which have been previously reported have good water solubility (~ 0.6 mg/mL) and to obtain a homogeneous and stable dispersion. In this work, we introduced OH-BNNS into DN hydrogel to obtain high thermal conductivity and toughness hydrogel. The DN hydrogel is a class of physically double-network hydrogel with hydrophobic association polyacrylamide (PAM) and partly crystalline polyvinyl alcohol (PVA). Impressively, the obtained PVA/PAM/BNNS composite hydrogel possesses super-flexibility, high toughness, good thermal conductivity, appropriate tissue adhesiveness and stimuli-free self-healing ability. Therefore, the composite hydrogel overcomes the poor mechanical strength and locally overheating issues as cartilage substitutes and may also become alternatives for antipyretic pastes.

Introduction

Hydrogel is a kind of polymer composite with water as a dispersed medium in which polymer forms 3D cross-linked network to hold water. They have been used in many fields because of high water content and biocompatibility, such as tissue engineering [1, 2], artificial cartilage [3, 4], actuator [5, 6] and wound dressing [7, 8]. However, their mechanical strength and toughness fail to meet the demand for practical application. Therefore, many researches on improvement in strength and toughness have been put forward, such as DN hydrogels [9, 10], nanocomposite hydrogels [11, 12], slide-ring hydrogels [13, 14] and macromolecular microsphere composite hydrogels [15, 16]. Among these methods, introducing the second network is an effective

Address correspondence to E-mail: ranrong@scu.edu.cn

https://doi.org/10.1007/s10853-018-3037-2

strategy to get tough DN hydrogel with high mechanical strength and toughness. For example, Gong et al. [9] prepared DN hydrogel with poly(2-acrylamido-2-methylpropane sulfonic acid sodium) (PAMPS) as the first network and PAM as the second network. The tensile and compressive strengths of obtained DN hydrogel were 0.69 MPa and 17.2 MPa, respectively, which were much higher than PAMPS or PAM single-network hydrogels. However, the chemically cross-linked DN hydrogel has the small elongation at break and no self-healing property. Self-healing property, a distinct characteristic of the natural biomaterial, refers to the ability to automatically reassemble and repair itself after being damaged from outside, and consequently enhance security as well as prolong functional lifetimes [17, 18]. Our previous report [19] has investigated a class of physically double-network (PDN) hydrogel with excellent self-healing property, which consisted of hydrophobic association (HA) PAM as the first network and partly crystalline PVA as the second network. Normally HA gels [20] are obtained by copolymerization of a hydrophilic monomer and a hydrophobic monomer under the action of a surfactant. The surfactants attract hydrophobic groups to form hydrophobically associated domains which act similarly to the cross-linkers in chemically linked hydrogels and promote polymer chains cross-linking, and thus, the gelation occurs and three-dimensional hydrogel networks are constructed. PVA hydrogel [21, 22] with high elasticity, prominent biocompatibility and superior lubricity has been the most promising candidate in biomaterials. PVA hydrogel occurs crystallization during the freeze–thawing process which is the main reason to improve the mechanical strength according to previous literature. Because of the fully physical cross-linked network, the hydrogel [19] reported in our previous work had good toughness and excellent self-healing property.

Although the above-mentioned achievements demonstrate the progress made, the fast development of robust and self-healing hydrogel calls for new requirements of performance. For example, local temperature increase resulting from the low heat transfer coefficient of the current polymer hydrogel has always led to poor mechanical properties and short lifetime [23–25]. Hexagonal boron nitrides (h-BNs) [26, 27] are often considered as a structural and isoelectronic analog of graphene, possessing ultimate thermal, chemical stabilities and mechanical strengths. However, h-BNs and derived boron nitride nanosheets (BNNSs) generally behave poor solubility not only in water but also in most organic solvents [28]. So the current major challenge is water soluble, especially in terms of their use in nanocomposite hydrogels. Several approaches [29–31] have been reported to improve the water solubility of the BNNS by introducing hydroxyl (-OH) or amido ($-NH_2$) functional groups onto their basal plane or edges, such as sonication-assistant exfoliation of bulk BN powder in water [32, 33], solution-phase oxygen radical functionalization of B atoms in the hexagonal BN lattice [34], heating BN powder in air [35], ball milling of BN powders in the presence of sodium hydroxide [36] and treating bulk BN powder with hot water steam [37]. But these OH-BNNSs were still limited to water-soluble and small lateral size which gone against thermal conductivity. Lin et al. [38] reported a remarkable approach to functionally modifying BN and thus got OH-BNNS with high water solubility (up to 0.6 mg/mL) and large lateral size ($\sim$ 2–3 μm) via two-step chemical oxidation and subsequent exfoliation processes. The as-prepared OH-BNNSs were evenly distributed in the hydrogel. On the one hand, the intrinsical hardness and high thermal conductivity of OH-BNNS give the composite hydrogel excellent mechanical toughness and thermal conductivity. On the other hand, the extraordinary network structure and hydrogen bonding interactions between the OH-BNNS and polymer chains play an important role in improving the performance of hydrogel.

In this paper, the OH-BNNS was introduced to PAM/PVA PDN hydrogel in which PAM was cross-linked by hydrophobic association microregion consisting of hydrophobic monomer (SMA) and surfactant (SDBS) and PVA was cross-linked by crystalline domain via cyclic freezing/thawing. The OH-BNNS after two-step chemical oxidation and exfoliation can be dispersed uniformly in the hydrogel without aggregation. In the presence of O, N and H on the polymer backbones and OH-BNNS, there will be much more hydrogen bonds between polymer chains and OH-BNNS. The hydrophobic associations and abundant hydrogen bonds can be reformed without any stimulation. As a result, the hydrogels could self-heal under room temperature. The mechanical behavior and thermal conductivity make a difference as the concentrations of PVA and OH-BNNS change. The PAM/PVA/BNNS hydrogel (with 0.4 wt% OH-

BNNS) achieved remarkably enhanced thermal conductivity from 0.33 to 0.47 W/(m K) (42% improvement). Impressively, the PAM/PVA/BNNS hydrogel showed moderate cohesive force with skins. Thus, the PAM/PVA/BNNS hydrogels with outstanding performance are expected to be promising candidates in antipyretic paste and cartilage replacement.

Experimental methods

Materials

Commercially hexagonal boron nitride (h-BN) was purchased from Ya'an Bestry Performance Materials Stock Co., Ltd. H_2SO_4 (98%) and HCl (37%) were provided by Xilong science Co., Ltd. $KMnO_4$ (99.5%) was purchased from Chengdu Kelong Chemical Reagent Factory. A total of 30 wt% H_2O_2 and P_2O_5 were purchased from Chengdu Jinshan Chemical Reagent Co., Ltd. Acrylamide (AM), PVA(1799) and sodium dodecyl benzene sulfonate (SDBS) were purchased from Aladdin Reagent Co., Ltd. Potassium persulfate (KPS) was purchased from Tianjin Bodi Chemical Co., Ltd., and was recrystallized from distilled water. Stearyl methylacrylate (SMA) was obtained from J&K Chemical Technology Co., Ltd., and used without further purification.

Preparation of OH-BNNS

The route to functionalize h-BN is similar to the previous work [38]. In brief, we firstly put 3 g h-BN, 2.5 g $K_2S_2O_8$ and 2.5 g P_2O_5 into concentrated H_2SO_4 (12 mL). The mixture was stirred for 4.5 h under 80 °C to complete the preoxidization. After filtered and washed, the preoxidized h-BN was dried at room temperature. Next, the h-BN was added into concentrated H_2SO_4 of the ice bath, stirring vigorously, and 15 g $KMnO_4$ was slowly added. After that, the mixture was heated 35 °C, reacting 2 h, and gradually added 250 mL water under another 2-h stirring. Finally, adding water and 30 wt% H_2O_2 to terminate the reaction, the resultant white color mixture was filtered and washed with 10 wt% HCl solution. Finally, the OH-BN was exfoliated in the water by ultrasonication for 1 h, which was followed by a 3000 rpm/min centrifugation to get rid of aggregated particles. A stable OH-BNNS suspension with a concentration of ~ 0.6 mg/mL was obtained.

Fabrication of PVA/PAM/BNNS hydrogel

First, adding PVA powder (1.5 g) in water to get a 5 wt% PVA solution and then refluxed at ~ 95 °C for 3 h. Then, different quantities of OH-BNNS aqueous solution (~ 0.6 mg/mL) (see Table S1 for more details) were introduced into the as-prepared PVA solution, and ultrasonic treatment at 60 °C for 1 h. Then, SDBS and SMA were added into the PVA/OH-BNNS solution with ultrasonic bathed at 50 °C for 0.5 h to get rid of air bubbles and dissolve SMA. The mixture was stirred for 2 h to fully dissolve the solid reagents and form hydrophobic association micelles. Next, we put AM and KPS into the mixture under 0.5-h stirring to get homogeneous solution. Finally, the solution was quickly transferred to the glass molds and put them into oven at 60 °C for 6 h to complete polymerization. There are two kinds of glass molds: (1) consisting of two rectangular glass panes separated by a 3-mm silicone rubber as a spacer. The hydrogel of this mold was sheet-like and then was cut into dumbbell-shaped using knife for tensile test. (2) a cylindrical bottle with a diameter of 20 mm. These resultant hydrogels were frozen to − 15 °C for 10 h and then thawed at room temperature for at least 12 h. After three freezing/thawing cycles, the crystalline physically PVA/PAM/BNNS hydrogel was obtained. These hydrogels with different shapes were prepared for subsequent characterization and tests. In this paper, composite hydrogels are designated as PVA_x/PAM/$BNNS_y$, where x stands for the relative mass fraction of PVA to the total weight and y stands for the different volume of OH-BNNS aqueous solution. PVA/PAM/$BNNS_y$ stands for the sample that the relative mass fraction of PVA to the total weight is 5%. The specific formula is shown in Table S1.

Characterization

Fourier transform infrared spectroscopy (FT-IR) spectra of h-BN, OH-BNNS, the PVA/PAM gel and OH-BNNS/PVA/PAM gels were recorded on a Nicolet6700 (Thermal Scientific, USA) spectrometer. The X-ray diffraction (XRD) measurements were performed at room temperature with a D/MAX 2400 X-ray diffractometer. The morphologies of h-BN, OH-BNNS, the PVA/PAM gel and PVA/PAM/BNNS gels were examined by a Quanta 250 scanning electron microscope (SEM) (FEI, USA) at 20 kV

acceleration voltage. The morphologies of OH-BNNSs were examined by a transmission electron microscopy (TEM) (Tecnai G2 F20, USA) at 200 kV.

Mechanical testing

Rheology measurements of the hydrogels were conducted with a TA AR2000ex rheometer using a parallel plate of diameter 20 mm. The hydrogels were cut into about 5-mm-thick wafers, and the frequency sweep was performed from 0.1 to 100 rad s^{-1} at a fixed strain of 1% at 25 °C.

Uniaxial tensile measurements of the hydrogels were performed using an Instron 5965 universal testing system with a 1 kN load cell at a crosshead speed of 100 mm min^{-1}, and the initial gauge length was 20 mm. Loading–unloading tensile measurements were stretched to a maximum strain of 800% and then unloaded. Energy dissipation capacity was estimated by the area of hysteresis loop. The compressive tests of the hydrogels were carried out by using the same testing system at a speed of 5 mm min^{-1}, and the gels were compressed to a maximum strain of 90%.

Thermal diffusivity/conductivity measurement

Thermal conductivity and diffusivity of the composite hydrogel samples with different OH-BNNS contents were measured using the transient plane source method (TPS 2500 S, Hot Disk, Gothenburg, Sweden) in accordance with the ISO 22007-2.2. During the measurement, a 2.001-mm-diameter C7577 TPS sensor was placed between the flat surfaces of two identical hydrogel samples (20 mm in diameter, 2.5 mm in thickness) at room temperature. The power output from the sensor heated up the samples, after which the electrical resistance of the sensor was monitored to determine the transient temperature. The sensor was assumed to be in an infinite sample medium for the subsequent analysis as the experimental measurement time is shorter as compared to the characteristic thermal diffusion time. Finally, the thermal conductivity and diffusivity parameters of the samples were calculated by successively iterating the detected transient temperatures. Multiple (at least 5) measurements were done for each sample to confirm the reproducibility.

As a supplement, we also measured the thermal conductivity of the hydrogel under wet conditions. The sheet-like hydrogels were spread on a hot plate at 50 °C, and the infrared imager was used to measure the temperature on the other side of the hydrogel, which can be used to evaluate the thermal conductivity of the hydrogels.

Result and discussion

Preparation and characterization of OH-BNNS

Commercial h-BN is generally not used for the preparation of hydrogels due to its poor water solubility. In this paper, h-BN was functionalized by a two-step oxidation process that was preoxidized using $K_2S_2O_8$ and P_2O_5 as oxidant, then $KMnO_4$ as oxidant for further oxidation to produce hydrogen bonds between hydroxyl groups at the edges and water to promote dissolution in water (Fig. 1a [38]). After oxidation, the OH-BNNS was divided into single- or few-layered nanosheets via liquid-phase sonication treatment. SEM and TEM were used to observe the morphology of h-BN and OH-BNNS (Fig. 1b–d). As we can see, the h-BN became more transparent under SEM after oxidation and exfoliation because the sheets of BN were thinner. An individual OH-BNNS layer had a lateral size of $\sim$ 2–4 μm which was consistent with TEM results. It is noted that the larger lateral size of the as-prepared OH-BNNS is beneficial for effective thermal and mechanical reinforcements. Besides, the TEM result showed that the edge of the obtained OH-BNNS was curled due to the thin layer which further demonstrated the successful exfoliation of OH-BNNS from bulk h-BN. In contrast to bulk h-BN, the OH-BNNS showed better hydrophilicity. The extremely poor solubility of the bulk h-BN in aqueous media is shown in Figure S1a. The bulk h-BN was deposited on the bottom of the bottle. However, the OH-BNNS could be uniformly dispersed in water and no aggregation occurred within 30 days. This can be explained by the fact that the introduction of –OH at the edge of OH-BNNS promoted interaction between OH-BNNS and water via hydrogen bonds. In addition, the OH-BNNS aqueous solution displayed an obvious Tyndall effect (Figure S1b) suggesting the successful exfoliation of the OH-BNNS. The FT-IR

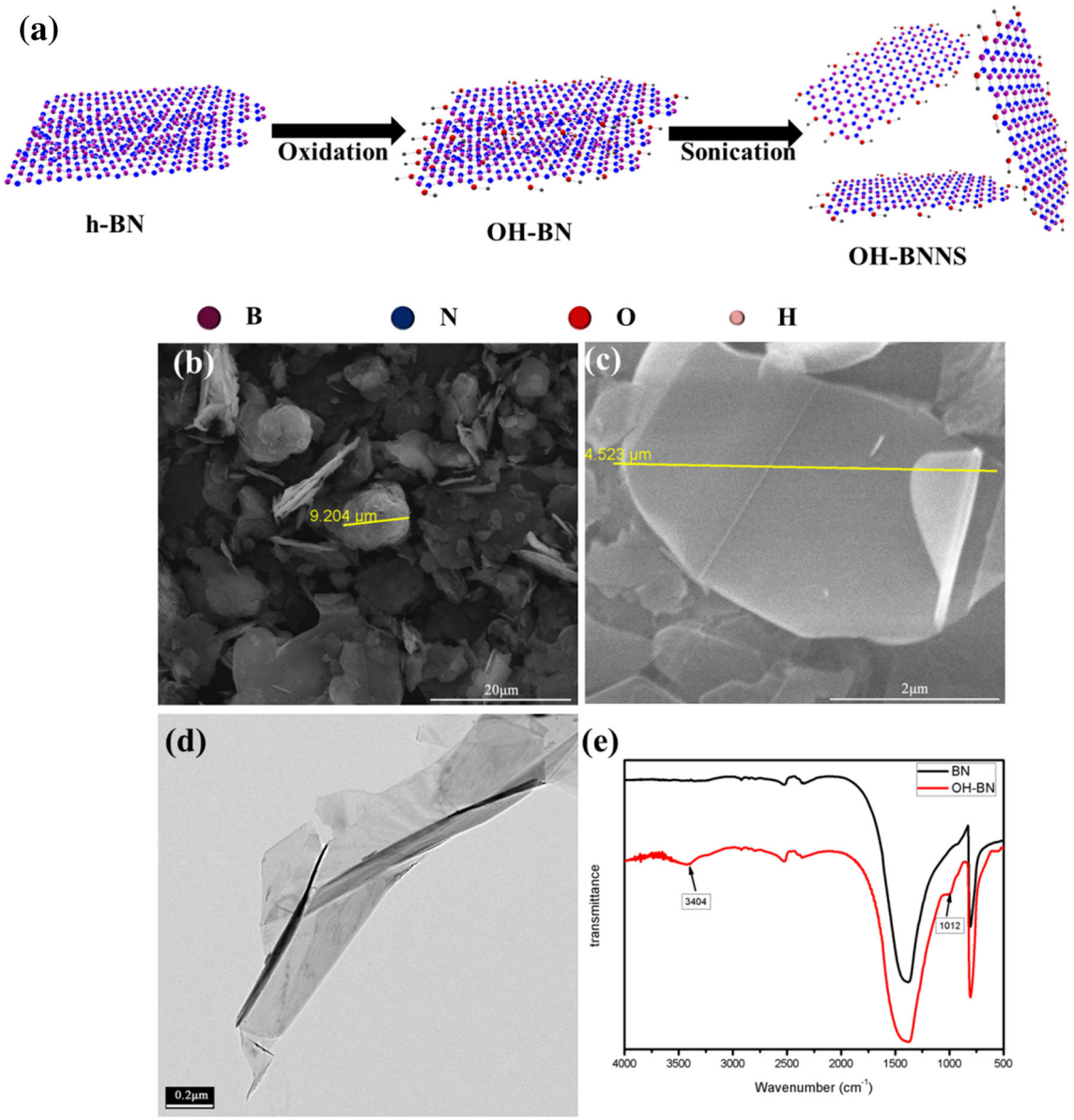

Figure 1 **a** Schematic illustration of synthesis route of the OH-BNNS; **b** SEM images of h-BN and **c** OH-BNNS; **d** TEM images of OH-BNNS; **e** FT-IR spectra of BN and OH-BNNS powders.

spectra of bulk h-BN and OH-BNNS also proved the effective functionalization after oxidation. Compared to the bulk h-BN, –OH stretching at 3404 cm^{-1} and B-O at 1012 cm^{-1} can be clearly seen in FT-IR spectra curve of the OH-BNNS, confirming the –OH functionalization of the BNNS. In order to characterize the stability of the nanosheets within the hydrogels, we observed the OH-BNNS dispersion after soaking in hot water at 60 °C for 6 h. As shown in Figure S2, we found that the nanosheets retained its hydrophilic and didn't precipitate at the bottom of the bottle. The temperature of OH-BNNS dispersion was 47 °C (below 60 °C) because of the cold environment. These results testified that the nanosheets had good stability after polymerization of AM at 60 °C. In other words, the nanosheets behave good stability within the hydrogels.

Preparation and characterization of hydrogels

The hydrogels with different contents of OH-BNNS were prepared by in situ polymerization (see "Experimental methods section" for more details). The

obtained hydrogels lost transparency due to the presence of boron nitride and partial crystallization of PVA after three freezing/thawing cycles (Fig. 2a). Various shapes hydrogels can be prepared by pouring the precursor solution into different molds. In this work, the chosen hydrophobic association network was the HAPAM gel and its "precursor" was dissolved PVA/OH-BNNS mixed aqueous solution. Then the PVA/PAM/BNNS hydrogels were prepared by in situ polymerization of AM in the PVA/OH-BNNS mixed aqueous solution. In addition to cross-linking of HAPAM gel themselves, cross-linking between PVA and PAM occurs through hydrogen bonds between OH-BNNS and PVA or PAM. In this way, the obtained DN composite hydrogel dissipates more energy to prevent their destruction under external forces.

FT-IR confirms existence of OH-BNNS in the PVA/PAM/BNNS hydrogels (Fig. 2b). In FT-IR spectra of PVA/PAM/$BNNS_4$ hydrogels, the characteristic peak of –OH shifted from 3431 to 3425 cm^{-1}, indicating that hydrogen bonds were formed between OH-BNNS and PVA or PAM. The peaks at 3200 cm^{-1} and 1651 cm^{-1} were assigned to the stretching vibration of N–H, C=O stretching in PAM. A peak at 2923 cm^{-1} was assigned to the $–CH_2$ groups, which were extensive in the polymer backbone. In addition, a weaker peak at 1016 cm^{-1} was the deformation vibration of B-O, which was consistent with the appearance of the OH-BNNS (Fig. 1e). These results

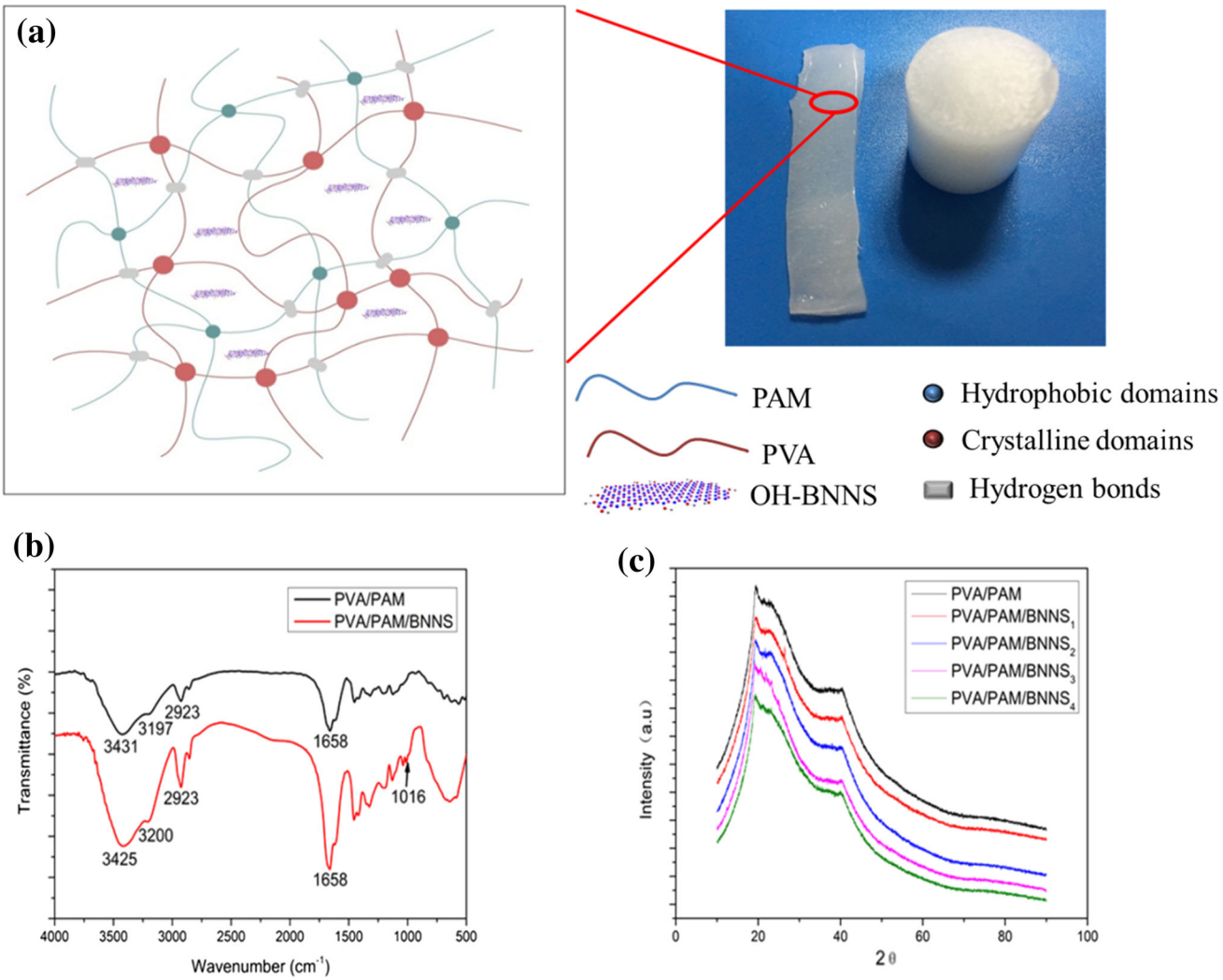

Figure 2 **a** Digital photograph of as-prepared sheet-like and cylindrical hydrogels and schematic illustration of hydrogel network structure. **b** FT-IR spectra of PVA/PAM and PVA/PAM/$BNNS_4$ hydrogels. **c** XRD patterns of hydrogels after three cycles of freezing/thawing treatment.

certified that PVA/PAM/BNNS hydrogels were prepared successfully.

It is known that for pure PVA several cycles of freezing/thawing treatment result in stable crystalline microdomains and higher crystallinity. This has been confirmed to be the case for the PVA/PAM/BNNS hydrogels as well. The X-ray diffraction measurement results of the PVA/PAM/BNNS hydrogels are shown in Fig. 2c. A sharp diffraction peak at $2\theta = 19.2°$ proved that the partially crystalline areas of PVA were formed after cycles of freezing/thawing. After adding different contents of OH-BNNS, the diffraction peak of the samples hardly changed. It shows that the relatively low amount addition of OH-BNNS will not affect the crystallization behavior of PVA.

The structural morphology of the PVA/PAM/BNNS hydrogels was directly acquired by SEM observations (Fig. 3). In order to facilitate the observation of the pore structure inside the gels, we first immersed the hydrogels in water for 30 min to swell and then freeze-dried for observation. Within the sample without OH-BNNS, the wall of the pore was shrunk to a certain degree due to poor stability. While PVA/PAM/BNNS hydrogels showed a much denser homogeneous structure with well-defined pores, the smooth pore wall adsorbed white OH-BNNSs particles and fibrous filaments at the cross section. Observably, the introduction of OH-BNNS showed a dramatic influence on the diameter of the pores in the hydrogels. The existence of OH-BNNS resulted in a significant decrease in diameter, which indicated that a more compact network structure was generated in PVA/PAM/BNNS gel by hydrogen bonds between OH-BNNS and PVA or PAM. Furthermore, the SEM–EDS images of PVA/PAM/$BNNS_2$ (Fig. S3) showed that the B and N elements were evenly distributed inside the gel, suggesting that OH-BNNS was uniformly dispersed in the hydrogel instead of agglomeration during the in situ polymerization of AM. This has a crucial role in improving the mechanical strength and thermal conductivity of hydrogels. Therefore, when loaded, more effective energy dissipation could be achieved by DN network and hydrogen bonds in the PVA/PAM/BNNS gel, resulting in an improvement in mechanical properties, which is consistent with Fig. 4. As a hydrogel, we have also tested the water content. The results are shown in Figure S4.

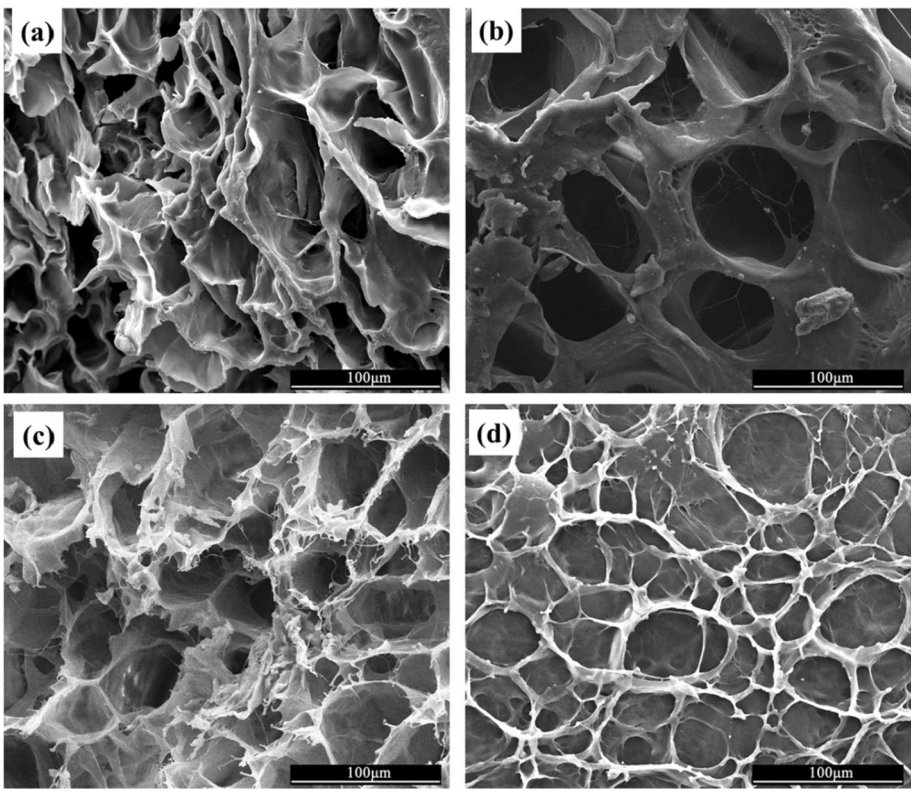

Figure 3 SEM images of PVA/PAM (**a**), PVA/PAM/$BNNS_1$ (**b**), PVA/PAM/$BNNS_3$ (**c**) and PVA/PAM/$BNNS_4$ (**d**).

Mechanical properties of hydrogels

Firstly, the mechanical behavior of the composite hydrogel has been investigated by dynamic rheological shear testing. It can be seen from Fig. S5 that the energy storage modulus (G′) of hydrogels was higher than the energy consumption modulus ("G") and appeared as almost a plateau over the experimental frequency range, which was evidence of the formation of cross-linked networks in these hydrogels.

Then the mechanical performance of hydrogels was tested via compressive and tensile tests. As shown in Fig. 4a, hydrogels can be stretched several times than their original length without breaking. Obviously, the tensile strength of the PVA/PAM/BNNS hydrogel first increased and then decreased with the increase in OH-BNNS content. When the content of OH-BNNS was 0.02 wt% (relative to hydrogels), the breaking strength of the hydrogel reached the highest value (~ 0.30 MPa). This is due to the fact that the addition of OH-BNNS makes the formation of hydrogen bonds between hydroxyl groups on OH-BNNS and –OH in PVA or $–NH_2$ in PAM. This stronger interaction makes the 3D network inside the hydrogel more closely entangled, while the pore size inside the gel is smaller (consistent with the SEM results). However, the fracture strength of gels began to decrease with the OH-BNNS content further increasing, which can be explained by the aggregation of excessive OH-BNNS in the hydrogel causing stress concentration. By integrating the stress–strain curves in Fig. 4d, the fracture strength and fracture energy of different samples are summarized in Fig. 4e. It was found that the fracture energy and strength had the same trend of change. And the highest fracture energy reached 1.1615 MJ/m^3 at 0.02 wt% OH-BNNS content. However, the

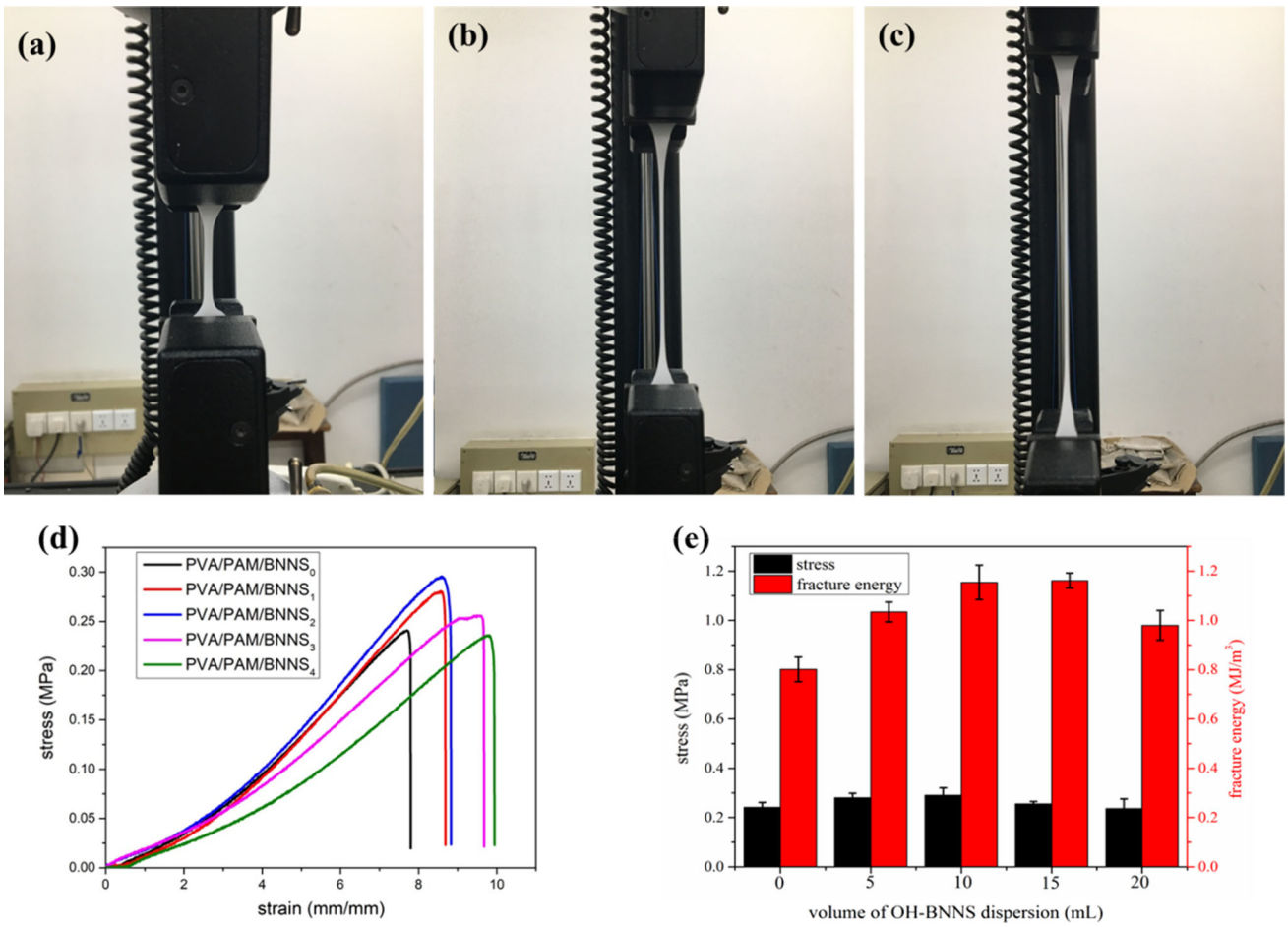

Figure 4 Digital photograph of hydrogel stretching process (**a**–**c**). Stress–strain curves (**d**) and stress and fracture energy (**e**) for PVA/PAM and PVA/PAM/BNNS hydrogels with different OH-BNNS contents.

elongation at break of the gels was consistently increasing with the OH-BNNS content increase. There are obvious hysteresis loops after loading–unloading tensile measurements (Fig. 5), which demonstrate that the hydrogel dissipates energy during stretching. In addition, the effect of PVA concentration on the mechanical strength of the hydrogel was also studied. It can be seen from Fig. S6 that as the content of PVA increases, both the tensile strength and the elongation of the hydrogel increased significantly.

Finally, compression tests further demonstrated the strong mechanical strength of PVA/PAM/BNNS hydrogel. As shown in Fig. 6b, the hydrogel can be compressed to 90% deformation without damage. When the external force is removed, the hydrogel can quickly (within 10 s) return to more than 80% of its original height (Fig. 6c). This fact shows that the gel has good rebound ability because of robust physical cross-linking in 3D networks. The high resilience demonstrates the reusability of the hydrogel. The compressive stress (Fig. 6d, e) of composite hydrogels was significantly enhanced and increased with the increase in OH-BNNS content. Compression stress of PVA/PAM/$BNNS_2$ reached ~ 2.77 MPa (at the strain of 90%), which was higher than PVA/PAM hydrogel (~ 2.06 MPa at the strain of 90%). Figure 6e is a partial view of compression stress–strain curves at the strain of 80–90%. Consistent with tensile strength results, the compressive strength of the hydrogel was reduced with the further addition of OH-BNNS.

Thermal diffusivity/conductivity of hydrogels

Continuous load-bearing and friction will cause heat accumulation in the cartilage tissue, so OH-BNNSs have been introduced to improve the thermal conductivity and diffusivity of the hydrogel. Hence, the PVA/PAM/BNNS hydrogel may have a great potential as a competitive candidate for articular cartilage. It is well known that uniformly dispersion of OH-BNNS is beneficial to thermal conductivity and diffusion. In this paper, the thermal conductivity of the gel under both dry and wet conditions was studied. Thermal conductivity and diffusivity of the composite gel were measured using the transient plane source method (see in Fig. 7) under dry condition. As the content of OH-BNNS increases, both the thermal conductivity and the heat-dissipating ability of the hydrogel increase. When the content of OH-BNNS was 0.04 wt% (relative to hydrogels), the thermal conductivity was 0.47 W/(mK), with an increase of 43.3% compared to the sample without OH-BNNS [0.33 W/(mK)]. At the same time, the thermal diffusivity of gels increased from 0.14 to 0.24 mm^2/s (increased about 71.4%) with the increase in the OH-BNNS content. In addition to the inherently high thermal conductivity of OH-BNNS, the polymer chains (PVA and PAM) and OH-BNNS in

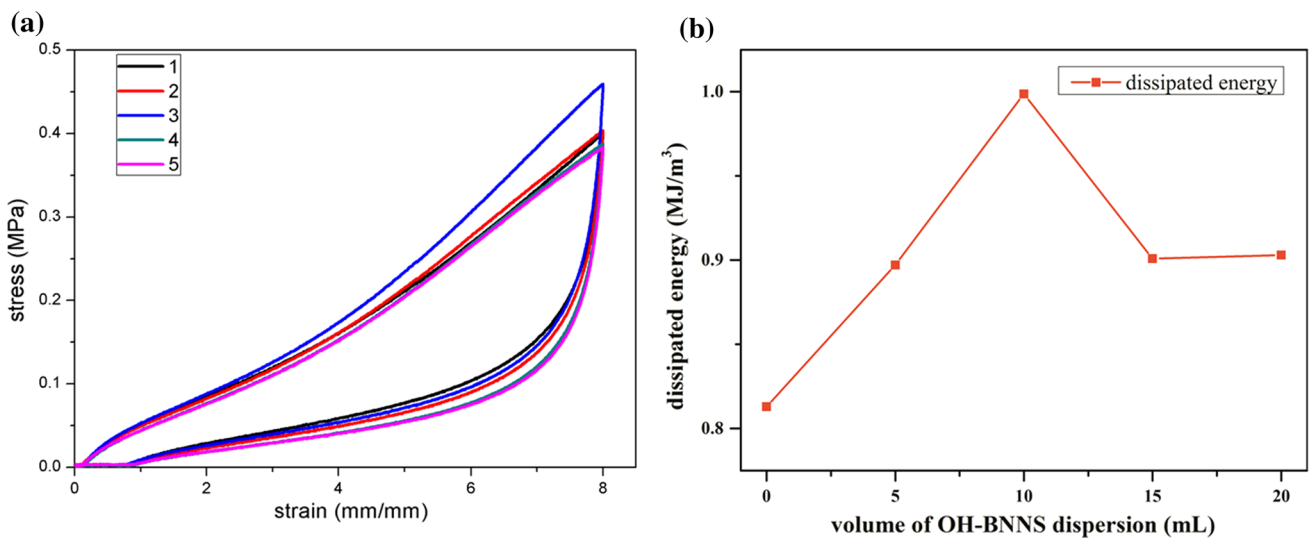

Figure 5 Loading–unloading stress–strain curves (**a**) and dissipated energy (**b**) for PVA/PAM and PVA/PAM/BNNS hydrogels with different OH-BNNS contents.

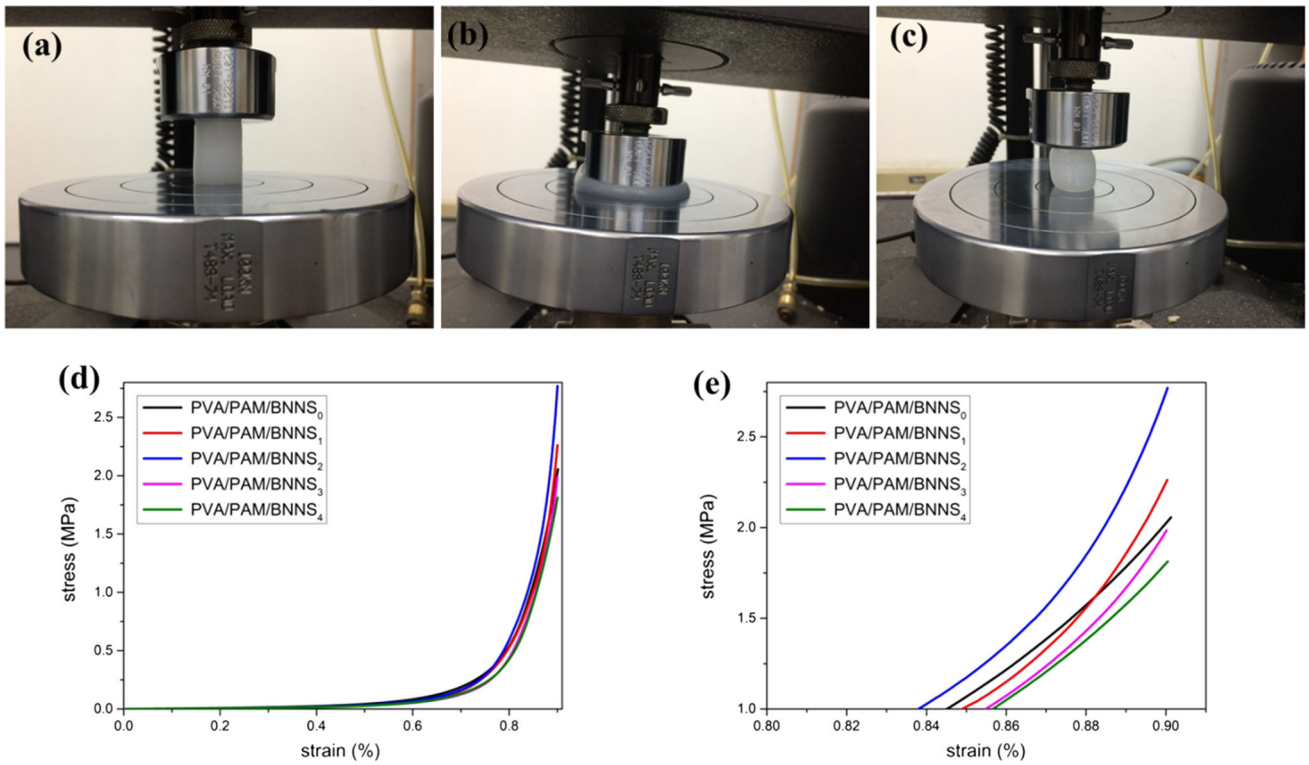

Figure 6 Digital photograph of hydrogel compression process (**a**–**c**). Compression stress–strain curves (**d**) for PVA/PAM and PVA/PAM/BNNS hydrogels with different OH-BNNS contents. Partial view (at the strain of 80–90%) (**e**) of compression stress–strain curves.

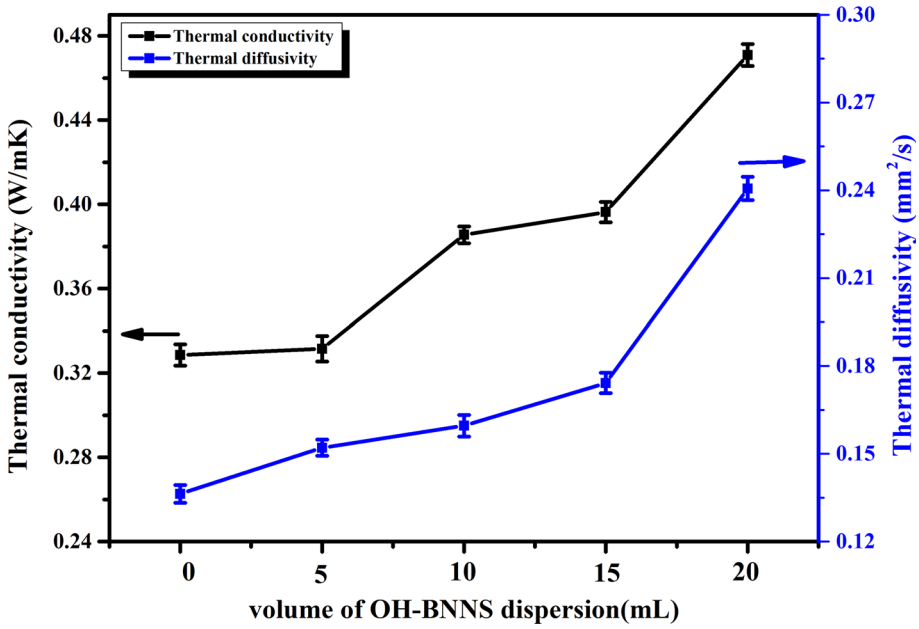

Figure 7 Thermal diffusivity/conductivity of PVA/PAM and PVA/PAM/BNNS hydrogels with different OH-BNNS contents.

the hydrogel form a brick–mud structure that provides an effective channel for heat conduction. The homogeneously dispersed OH-BNNS acts as a brick portion, while the flexible polymer chains act as a mud portion, which is firmly bonded together by hydrogen bonds, thus minimizing heat conduction resistance. Furthermore, the thermal conductivity of hydrogels under water-containing conditions was also studied using an infrared imager. As shown in Fig. 8a, the hydrogels were placed on a glass plate on

a hot stage (50 °C) and after 30 s the temperature of the upper surface increased with increasing OH-BNNS content. The sample centered on the stage was the sample without OH-BNNS added. The content of OH-BNNS increased sequentially from the upper right corner to lower right corner along a counter-clockwise direction. In the same period of time, the higher the OH-BNNS content was, the higher the temperature reached, and the highest temperature reached 44.1 °C (Fig. 8b). While the area of the region where the hydrogel temperature rose enlarged with the increase in OH-BNNS content, indicating that the more OH-BNNS content the better heat dissipation capability was.

In addition, the effect of PVA content on the thermal conductivity of hydrogels was also studied (Fig. S7). When the PVA content was 5%, the hot spot temperature was 43.7 °C, which was higher than the sample without PVA. After the amount of PVA had been further increased, the temperature of the sample surface began to decrease. One reason is that the excessive PVA causes the expansion of volume between OH-BNNSs. Another reason is that the more PVA crystal microdomain resulted in more diffusion energy. In conclusion, the PVA/PAM/BNNS hydrogels had good thermal conductivity and diffusivity, so we expect that the hydrogel may be capable to be used as antipyretic pastes and artificial cartilage.

Cohesiveness and self-healing of hydrogels

Hydrogels with high heat-conducting and heat-dissipating capabilities can be used as antipyretic pastes to reduce the temperature. However, the hydrogels should also have a suitable adhesion to the skin [39, 40]. When the adhesive force is too large, the human body feels pain when peeled from the skin, and there may be some residue on the skin after peeling. If the adhesive strength is too small, it is not enough to fix the adhesion of the hydrogel itself to the skin, which may cause inconvenience in use. Amazingly, the PVA/PAM/BNNS hydrogel is able to adhere to human skin with no irritation and could be removed easily without causing any damage or pain. As shown in Fig. 9, the hydrogel can stick to the skin without falling down, although the side of the hydrogel downwards. And no matter how we shake our wrists, there's no separation between the hydrogel and the skin. The mechanism of the tissue adhesiveness of the hydrogel may rely on the physical interaction, such as hydrogen bond, Van der Waals forces, π-π stacking interaction or several synergetic interactions which simultaneously exist between hydrogel and skin [30]. There was no residue after peeling from the skin. More importantly, the PVA, BNNS and main material of hydrogel showed biocompatibility and low toxicity [38, 39]. We believe that the hydrogel may be potential material as antipyretic pastes for children or adults. Meanwhile, the as-prepared hydrogels possess the ability to self-heal due to fully physical cross-linking such as hydrogen

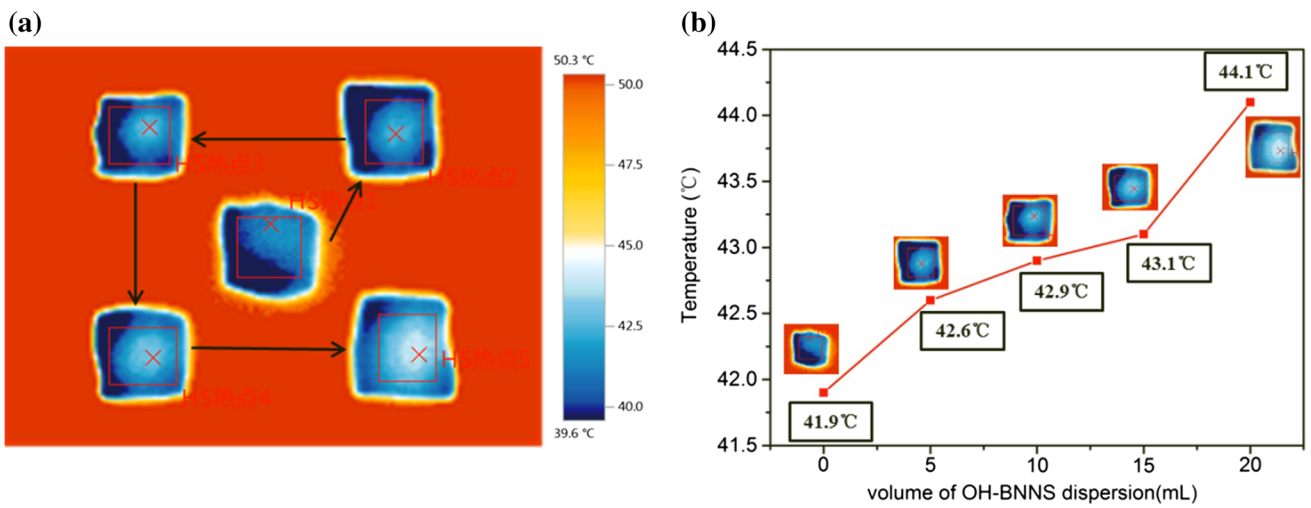

Figure 8 **a** Thermal-infrared images (the content of OH-BNNS increases along the arrow) and **b** hot spots of PVA/PAM and PVA/PAM/BNNS hydrogels with different OH-BNNS contents.

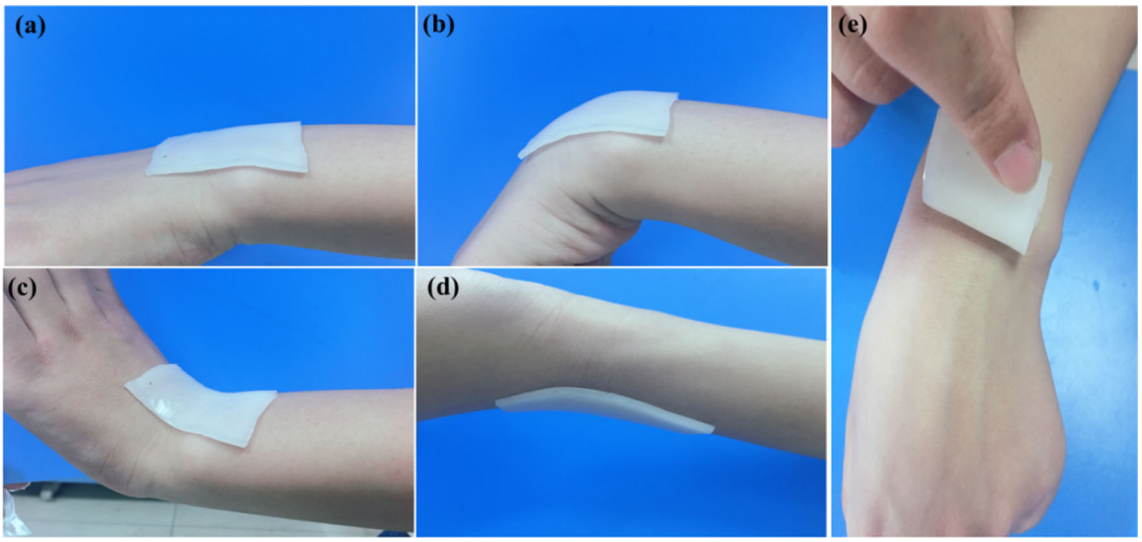

Figure 9 Tissue cohesiveness of PVA/PAM/$BNNS_2$ hydrogel. Hydrogel on the surface of the first author's wrist (**a**), bending wrists up (**b**) and down (**c**), overturn wrist (**d**) without falling down. (**e**) No residue after peeling from skin.

bonds, hydrophobic association and molecular chain entanglement. As we can see in Fig. 10, the hydrogel was cut into two parts, then the two sections were placed together and self-healed in a sealed Petri dish at room temperature without any stimulation. After 15 h, it can be seen that the cracks in the middle of the hydrogel have completely disappeared, and the two parts didn't separate after pulling the self-healing hydrogel in the lateral direction. And the self-healing time was shortened after the temperature rises. In addition, we have charactered the self-healing efficiency of the hydrogel by uniaxial tensile measurements. As shown in Fig. 11, the fracture strength of the hydrogel after self-healing reached 0.22 MPa, and the strain was 710%. The self-healing efficiencies of strength and strain were 73.3% and 78.9%,

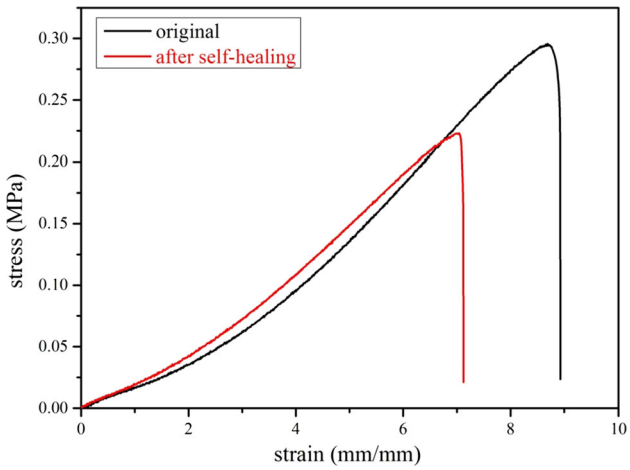

Figure 11 Stress–strain curves for PVA/PAM/$BNNS_2$ hydrogel and the hydrogel after self-healing.

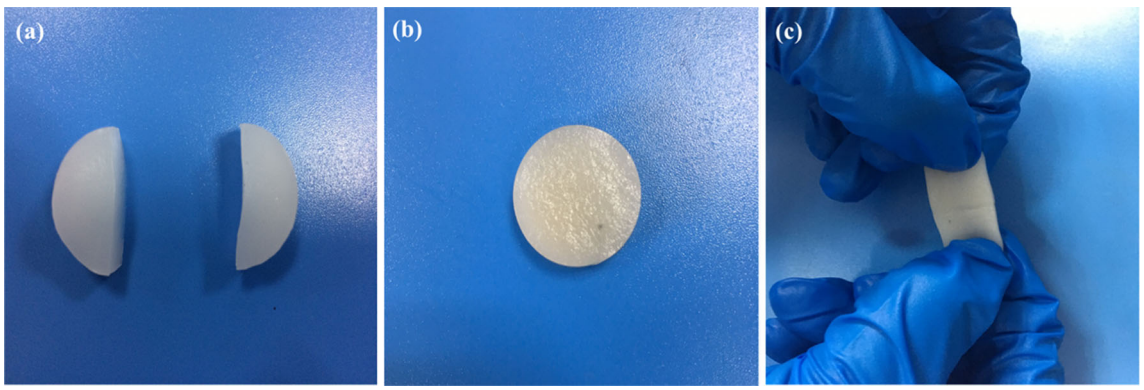

Figure 10 Self-healing of PVA/PAM/$BNNS_2$ hydrogel. **a** Hydrogel was cut into two parts, **b** self-healed at room temperature, **c** pulling the hydrogel after self-healing.

respectively. These results demonstrate that the hydrogels possess good self-healing ability. The cracks in the middle of hydrogel have completely disappeared after self-healing 5 h at 60 °C. This is due to the more flexible mobility of polymer molecular chains under higher temperature conditions. These results demonstrate again that the high thermal conductivity and mechanical strength hydrogels are suitable substitute materials for antipyretic pastes or cartilage tissue.

Conclusion

In summary, we have successfully functionalized boron nitride into OH-BNNS, then introduced OH-BNNS into PVA and PAM double-network hydrogels via in situ polymerization. The characterization data indicated that OH-BNNS was uniformly dispersed in the hydrogel, and formed a unique network structure with polymer chains. So, the as-prepared hydrogel has higher thermal conductivity and mechanical strength. The highest tensile strength and fracture energy of the PVA/PAM/$BNNS_2$ (adding 0.02 wt% OH-BNNS) hydrogel reached ~ 0.30 MPa and 1.1615 MJ/m^3. The compression stress of PVA/PAM/$BNNS_2$ hydrogel reached ~ 2.77 MPa (at the strain of 90%). What's more, the mechanical strength can also be adjusted by changing the content of PVA. Importantly, the results tested by transient plane source method and the thermal-infrared images under dry and wet condition, respectively, demonstrated that the hydrogels had better thermal conductivity and diffusivity as the content of OH-BNNS increased. Compared to the sample without OH-BNNS (0.33 W/mK), the thermal conductivity of PVA/PAM/$BNNS_4$ (adding 0.04 wt% OH-BNNS) composite hydrogel was 0.47 W/mK (an increase of 43.3%), and thermal diffusivity of gels varied from 0.14 to 0.24 mm^2/s (an increase of 71.4%). In addition, the hydrogel showed moderate adhesive force to skin, which is important for the use of antipyretic pastes. Moreover, the PVA/PAM/BNNS composite hydrogels possess the ability to self-heal due to fully physical cross-linking. The hydrogels with high mechanical properties and thermal conductivity are promising potential in the mechanical failure and locally overheating issues as cartilage substitutes and may also have broad utility for biomedical applications, such as antipyretic pastes, tissue engineering, biosensors and actuators.

Acknowledgements

This work was supported by National Natural Science Foundation of China (Grants 51773124, 51403132), Sichuan Science and Technology Program China (Grants 2016GZ0300, 2018GZ0322), Innovation Team Program of Science and Technology Department of Sichuan Province (Grant 2014TD0002), Cooperation strategic projects of Luzhou governments and Sichuan University (Grant 2015CDLZ-G13) and the Fundamental Research Funds for the Central Universities (Grant 2012017yjsy184).

Electronic supplementary material: The online version of this article (https://doi.org/10.1007/s10853-018-3037-2) contains supplementary material, which is available to authorized users.

References

[1] Lee KY, Mooney DJ (2001) Hydrogels for tissue engineering. Chem Rev 101(7):1869–1880

[2] Fisher SA, Tam RY, Shoichet MS (2014) Tissue mimetics: engineered hydrogel matrices provide biomimetic environments for cell growth. Tissue Eng Part A 20(5–6):895–898

[3] Baker MI, Walsh SP, Schwartz Z, Boyan BD (2012) A review of polyvinyl alcohol and its uses in cartilage and orthopedic applications. J Biomed Mater Res B Appl Biomater 100(5):1451–1457

[4] Ren KX, He CL, Xiao CS, Li G, Chen XS (2015) Injectable glycopolypeptide hydrogels as biomimetic scaffolds for cartilage tissue engineering. Biomaterials 51:238–249

[5] Dong L, Agarwal AK, Beebe DJ, Jiang H (2006) Adaptive liquid microlenses activated by stimuli-responsive hydrogels. Nature 442(7102):551–554

[6] Velders AH, Dijksman JA, Saggiomo V (2017) Hydrogel actuators as responsive instruments for cheap open technology (HARICOT). Appl Mater Today 9:271–275

[7] Lim S, Nguyen MP, Choi Y, Kim J, Kim D (2017) Bioadhesive nanoaggregates based on polyaspartamide-g-C18/DOPA for wound healing. Biomacromol 18(8):2402–2409

[8] Fan Z, Liu B, Wang J, Zhang S, Lin Q, Gong P, Ma L, Yang S (2014) A novel wound dressing based on Ag/graphene

polymer hydrogel: effectively kill bacteria and accelerate wound healing. Adv Func Mater 24(25):3933–3943

[9] Gong JP, Katsuyama Y, Kurokawa T, Osada Y (2003) Double-network hydrogels with extremely high mechanical strength. Adv Mater 15(14):1155–1158

[10] Dai X, Zhang Y, Gao L, Bai T, Wang W, Cui Y, Liu W (2015) A mechanically strong, highly stable, thermoplastic, and self-healable supramolecular polymer hydrogel. Adv Mater 27(23):3566–3571

[11] Zhu M, Liu Y, Sun B, Zhang W, Liu X, Yu H, Zhang Y, Kuckling D, Adler HJP (2006) A novel highly resilient nanocomposite hydrogel with low hysteresis and ultrahigh elongation. Macromol Rapid Commun 27(13):1023–1028

[12] Haraguchi K, Takehisa T (2002) Nanocomposite hydrogels: a unique organic–inorganic network structure with extraordinary mechanical, optical, and swelling/de-swelling properties. Adv Mater 14(16):1120–1124

[13] Okumura Y, Ito K (2001) The polyrotaxane gel: a topological gel by figure-of-eight cross-links. Adv Mater 13(7):485–487

[14] Guo M, Jiang M, Pispas S, Yu W, Zhou C (2008) Supramolecular hydrogels made of end-functionalized low-molecular-weight PEG and α-cyclodextrin and their hybridization with SiO_2 nanoparticles through host–guest interaction. Macromolecules 41(24):9744–9749

[15] Huang T, Xu H, Jiao K, Zhu L, Brown HR, Wang H (2007) A novel hydrogel with high mechanical strength: a macromolecular microsphere composite hydrogel. Adv Mater 19(12):1622–1626

[16] Zhao J, Jiao K, Yang J, He C, Wang H (2013) Mechanically strong and thermosensitive macromolecular microsphere composite poly (N-isopropylacrylamide) hydrogels. Polymer 54(6):1596–1602

[17] Nakahata M, Takashima Y, Yamaguchi H, Harada A (2011) Redox-responsive self-healing materials formed from host–guest polymers. Nature communications 2:511–517

[18] Yang Y, Urban MW (2013) Self-healing polymeric materials. Chem Soc Rev 42(17):7446–7467

[19] Zhang Y, Song M, Diao Y, Li B, Shi L, Ran R (2016) Preparation and properties of polyacrylamide/polyvinyl alcohol physical double network hydrogel. RSC Advances 6(113):112468–112476

[20] Tuncaboylu DC, Sari M, Oppermann W, Okay O (2011) Tough and self-healing hydrogels formed via hydrophobic interactions. Macromolecules 44(12):4997–5005

[21] Hassan CM, Peppas NA (2000) Structure and morphology of freeze/thawed PVA hydrogels. Macromolecules 33(7):2472–2479

[22] Li G, Zhang H, Fortin D, Xia H, Zhao Y (2015) Poly (vinyl alcohol)–poly (ethylene glycol) double-network hydrogel: a general approach to shape memory and self-healing functionalities. Langmuir 31(42):11709–11716

[23] Bali R, Sharma S (2011) A model for intra-articular heat exchange in a knee joint. Tribol Lett 41(2):379–386

[24] Abdel-Sayed P, Moghadam MN, Salomir R, Tchernin D, Pioletti DP (2014) Intrinsic viscoelasticity increases temperature in knee cartilage under physiological loading. J Mech Behav Biomed Mater 30:123–130

[25] Abdel-Sayed P, Darwiche SE, Kettenberger U, Pioletti DP (2014) The role of energy dissipation of polymeric scaffolds in the mechanobiological modulation of chondrogenic expression. Biomaterials 35(6):1890–1897

[26] Pakdel A, Bando Y, Golberg D (2014) Nano boron nitride flatland. Chem Soc Rev 43(3):934–959

[27] Lu F, Wang F, Cao L, Kong CY, Huang X (2012) Hexagonal boron nitride nanomaterials: advances towards bioapplications. Nanoscience and Nanotechnology Letters 4(10):949–961

[28] Ikuno T, Sainsbury T, Okawa D, Fréchet J, Zettl A (2007) Amine-functionalized boron nitride nanotubes. Solid State Commun 142(11):643–646

[29] Hu X, Liu J, He Q, Meng Y, Cao L, Sun Y-P, Chen J, Lu F (2016) Aqueous compatible boron nitride nanosheets for high-performance hydrogels. Nanoscale 8(7):4260–4266

[30] Tong X, Du L, Xu Q (2018) Tough, adhesive and self-healing conductive 3D network hydrogel of physically linked functionalized-boron nitride/clay/poly (N-isopropylacrylamide). Journal of Materials Chemistry A 6(7):3091–3099

[31] Xue S, Wu Y, Wang J, Guo M, Liu D, Lei W (2018) Boron nitride nanosheets/PNIPAM hydrogels with improved thermo-responsive performance. Materials (Basel, Switzerland) 11(7):1069–1078

[32] Lin Y, Williams TV, Connell JW (2009) Soluble, exfoliated hexagonal boron nitride nanosheets. J Phys Chem Lett 1(1):277–283

[33] Jiang H, Wang Z, Geng H, Song X, Zeng H, Zhi C (2017) Highly flexible and self-healable thermal interface material based on boron nitride nanosheets and a dual cross-linked hydrogel. ACS Appl Mater Interfaces 9(11):10078–10084

[34] Sainsbury T, Satti A, May P, Wang Z, McGovern I, Gun'ko YK, Coleman J (2012) Oxygen radical functionalization of boron nitride nanosheets. J Am Chem Soc 134(45):18758–18771

[35] Yu B, Xing W, Guo W, Qiu S, Wang X, Lo S, Hu Y (2016) Thermal exfoliation of hexagonal boron nitride for effective enhancements on thermal stability, flame retardancy and smoke suppression of epoxy resin nanocomposites via sol–gel process. J Mater Chem A 4(19):7330–7340

[36] Lee D, Lee B, Park KH, Ryu HJ, Jeon S, Hong SH (2015) Scalable exfoliation process for highly soluble boron nitride nanoplatelets by hydroxide-assisted ball milling. Nano Lett 15(2):1238–1244

[37] Xiao F, Naficy S, Casillas G, Khan MH, Katkus T, Jiang L, Liu H, Li H, Huang Z (2015) Edge-hydroxylated boron nitride nanosheets as an effective additive to improve the thermal response of hydrogels. Adv Mater 27(44):7196–7203

[38] Jing L, Li H, Tay RY, Sun B, Tsang SH, Cometto O, Lin J, Teo EHT, Tok AIY (2017) Biocompatible hydroxylated boron nitride nanosheets/poly (vinyl alcohol) interpenetrating hydrogels with enhanced mechanical and thermal responses. ACS Nano 11(4):3742–3751

[39] Han L, Lu X, Liu K, Wang K, Fang L, Weng L-T, Zhang H, Tang Y, Ren F, Zhao C (2017) Mussel-inspired adhesive and tough hydrogel based on nanoclay confined dopamine polymerization. ACS Nano 11(3):2561–2574

[40] Han L, Yan L, Wang K, Fang L, Zhang H, Tang Y, Ding Y, Weng L-T, Xu J, Weng J (2017) Tough, self-healable and tissue-adhesive hydrogel with tunable multifunctionality. NPG Asia Materials 9(4):e372–e384